Design of a Calorimeter for Measurement of Heat Generation Rate of Lithium Ion Battery Using Thermoelectric Device

Yilin Yin and Zhong Zheng
Auburn University

Song-Yul Choe
Auburn Univ.

ABSTRACT

Analysis of thermal behavior of Lithium ion battery is one of crucial issues to ensure a safe and durable operation. Temperature is the physical quantity that is widely used for analysis, but limited for accurate investigations of behavior of heat generation of battery because of sensitivities affected by heat transfer in experiments. Calorimeter available commercially is widely used to measure the heat generation of battery, but does not follow required dynamics because of a relatively large thermal time constant given by cavity and a limited heat transfer capability. In this paper, we proposed a highly dynamic calorimeter that was constructed using two thermoelectric devices (TEMs). For the design of the calorimeter and its calibration, a printed circuit board (PCB) with the same size as the battery was used as a dummy load to generate controlled heat. Dynamics were improved using a lead-lag compensator for temperature control and heat generation was estimated using Kalman filter based on a thermal model of the calorimeter. All parameters were optimized using the PCB. Finally, heat generation rate of a large format of pouch type lithium ion battery was measured and compared with theoretical values.

INTRODUCTION

As energy storage components, lithium ion batteries are widely used in electrical vehicles (EV) and grids because of its high coulombic efficiency, higher power and energy density, and long durability. When lithium ion batteries are charged and discharged, lithium ions flow from cathode to anode and vice versa through the electrolyte, while electrons are transported through an external circuit. The charge transport, chemical reaction, diffusion in the solid and Ohmic's heating produce heat [1], and at the same time, performances of battery are significantly affected by its operating temperature. Charging and discharging lithium ion battery in an elevated temperature accelerates its side reaction and leads to the electrolyte and binder decompositions and reduction of the accessible surface area of the electrode particles. So high operating temperature accelerates power and capacity fade of battery. Santhanagopalan's experiment results at the operating temperatures from 5°C to 45°C showed that the capacity fade of lithium ion battery at 45°C was nine times higher than that at 5°C [2]. And, to minimize the effects of elevated temperature on degradation and other performances and to prevent a thermal runaway, the large amount of heat generated by the battery in a pack or modules should be properly rejected [3]. In order to optimally reject the generated heat, accurate estimation the heat generation rate of lithium ion battery is needed, which is also crucial for its safe operations.

When battery is charged and discharged, the battery's temperature varies due to the internal heat generation [4,5] Heat generation in lithium ion battery consists of two main parts, the reversible heat generated by the change of entropy at a given cell temperature and irreversible heat generated by Joule heat, charge-transfer overpotentials and mass transfer limitations[6, 7]. The heat generation sources are difficult to be estimated based on the thermal model because of temperature-dependent parameters in the thermal model, the changing of electrode resistivity due to current and temperature effects, and the complex behavior of interfacial areas of the electrode and electrolyte[8,9]. Therefore, heat generation rate in the lithium ion battery is preferably measured directly using a calorimeter. There are two known methods: accelerated rate calorimetry (ARC) and isothermal heat conduction calorimetry (IHC) [9]. ARC method measures the heat generation rate of battery based on the increase of battery's temperature and the amount of heat released from the battery to the surroundings. Forgeza used two thermal couples to measure the heat generation rate. One thermal couple was placed into a cylindrical lithium ion battery under an inert atmosphere and another one was placed on the battery surface to measure both inside and outside temperatures [10, 11]. This method measures the heat generation rate accurately but only provides accurate results for the cylindrical batteries that can place a thermal couple inside of a cell. Hong's research team used an accelerated rate calorimeter (ARC2000, Columbia Scientific Industries, Austin, Texas) to

establish the baseline condition which is necessary for measuring the heat effects associated with discharging/charging the cells with the maximum measured heat generation rate of 1.63W/L [12]. However, the heat generation during charging and discharging is far beyond the measurement range of the calorimeter described before, and it is impossible to follow the dynamics of the heat generation rate that varies fast. The IHC method measures the heat generation rate by using a large heat sink that contacts the surface of the battery to keep the battery at isothermal conditions during measurement [13, 14]. Kim used a commercially available micro-calorimeter (IMC, CSC4400, Calorimetry Science Corp) to measure the heat generation rate of lithium ion battery. However, the IHC method can only measure low heat generation rate because the heat sink cannot extract high rate of heat generation. And, the limited dynamics prevent the measurement of the heat generation rate that changes fast because of a relatively larger thermal time constant.

The lithium ion batteries used for the studies have high power, which generates heat at a high rate during large charging/discharging C-rate.

Therefore, we designed a special calorimeter using two thermoelectric devices that can provide an accurate and fast measurement of the heat generation of the pouch type of lithium ion battery. The calorimeter was modeled and its parameters were identified. Lead-lag compensator was used to keep the temperature of surface of battery to be constant and heat generation was estimated using Kalman filter, which is described in detail below.

MODELING OF CALORIMETER

Calorimeters are commonly used to measure heat generation rate of different kinds of batteries, but they are unable to follow the dynamics of heat generation rate occurring during step or pulse charging and discharging of cells because of a relatively large thermal time constant. To solve the problem, a new special calorimeter was designed using two thermoelectric devices (TEMs).

TEMs are widely used as heat pump in many applications, which includes cooling or heating of an object in control loop [15,16,17]. For control purpose, a mathematical model of TEM was developed, which is a challenging issue because of the nonlinear behavior of TEM. Some researchers proposed a finite element model and finite difference model [18,19]. Neto presented a second order discrete time autoregressive moving average model to describe the TEM [20]. However, these model are too complex to be used to design the controller and heat estimation algorithm.

In this paper, we proposed a simple but accurate model considering the nonlinear characteristics of TEM, which was used to design the controller and heat generation estimation algorithm.

The key components in TEM are the semiconductors (P-N junctions), which are placed thermally in parallel to each other and electrically in series, as shown in Figure 1. The TEM works according to Peltier effect, which occurs whenever electrical current flows through P-N junctions. When a DC voltage is applied to the P-N junctions, the

electrons in the N junctions and the 'holes' in the P junctions move from cold side to the hot side and carry the heat from bottom junctions to the top junctions. Depending on the direction of current flow, the junctions either absorb or release heat, so that one side gets colder while the other gets hotter. The hot side is attached to a heat sink to accelerate the release of the heat, shown in Figure 2. The quantity of heat liberated by the holes and electrons per unit of time is proportional to the input current of TEM [22, 23].

$$Q_p = k_1 \cdot I_{TEM} = \alpha \cdot T_2 \cdot I_{TEM}$$

(1)

where k_1 is the Peltier coefficient, α is the Seebeck coefficient. T_2 is the absolute temperature of TEM (cold side). *ITEM* is the input current of TEM. When current flows through a conductor that has a temperature gradient, heat is absorbed or released depending on the direction of temperature gradient and direction of the current, which is called Thomson effect [24, 25].

$$Q_T = \tau \cdot I_{TEM} \cdot \frac{dT}{dx}$$

(2)

where τ is the Thomson coefficient and x is the space variable. In our design. The heat generated by Thomson effect is ignored because of the difficulty to measure and negligible amount compared to Joule effect [26].
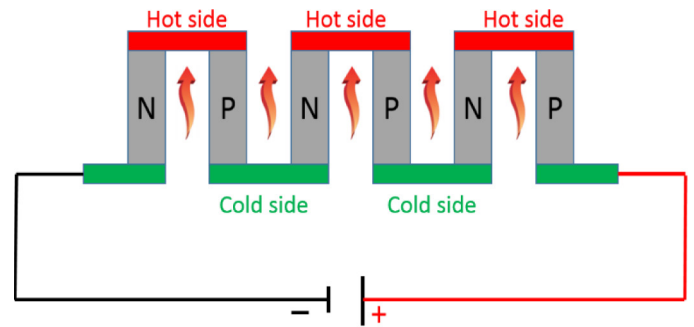

Figure 1. Working principle of TEM

When current flows into TEM, Joule heat is generated due to the resistance ($k2$) of P-N junctions inside of TEM,

$$Q_J = I_{TEM}^2 \cdot k_2$$

(3)

Temperature gradient exists between T_2 and T_3, so there is a heat conduction from the hot side (T_3) to the cold side (T_2),

$$Q_k = k_3(T_2 - T_3)$$

(4)

where k_3 is the thermal conduction coefficient. Finally, the heat pump rate of the TEM is given as follows,

$$Q_{pump} = k_1 \cdot I_{TEM} - k_2 I_{TEM}^2 + k_3(T_2 - T_3)$$

(5)

When the battery is charged or discharged using pulse or step current, especially for fast charging, the heat generation rate changes abruptly. The dynamics of the calorimeter are limited by the time delay between the input current of TEM and the associated heat pump rate. The dominant time delay is caused by the limited thermal conductivity and thermal capacitance of the metal plate, shown in Figure 2. In order to reduce the effects of the time delay, Kalman filter was used based on the heat transfer model of the calorimeter, which ultimately improves the dynamic response of the designed calorimeter.

The time delay is mainly caused by the metal plate, so only a thermal model of the metal plate was considered and developed. The metal plate is separated into two control volumes, as shown in Figure 3.
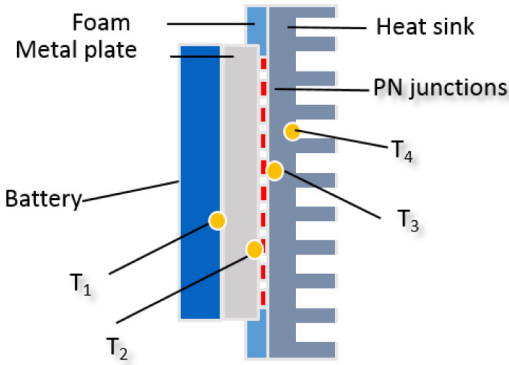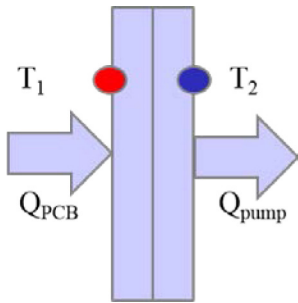

Figure 2. The structure of TEM

Figure 3. Control volumes of metal plates

Energy equations for the two control volumes of the metal plate is shown below,

$$\left.\begin{array}{l}(\frac{C_M M_M}{2})\dot{T}_1 = Q_{PCB} - K\ (T_1 - T_2) \\ (\frac{C_M M_M}{2})\dot{T}_2 = K\ (T_1 - T_2) - Q_{pump}\end{array}\right\}$$

$$(6)$$

where C_M is the heat capacity of the metal plate, M_M is the mass of metal plate, K the thermal conductivity of metal plate, Q_{pump} is the heat pump out by TEM. Q_{PCB} is the heat generated by the printed circuit board (PCB).

Using forward difference method, the discretized model of the equation above is written in matrix form as follows

$$\begin{bmatrix} T_1^{k+1} \\ T_2^{k+1} \end{bmatrix} = \begin{bmatrix} 1 - \frac{2K\Delta t}{C_M M_M} & \frac{2K\Delta t}{C_M M_M} \\ \frac{2K\Delta t}{C_M M_M} & 1 - \frac{2K\Delta t}{C_M M_M} \end{bmatrix} \begin{bmatrix} T_1^k \\ T_2^k \end{bmatrix} + \begin{bmatrix} \frac{2K\Delta t}{C_M M_M} & \frac{2K\Delta t}{C_M M_M} \\ -2K\Delta t & \frac{-2K\Delta t}{C_M M_M} \end{bmatrix} \begin{bmatrix} Q_{PCB} \\ Q_{pump} \end{bmatrix}$$

$$(7)$$

In order to design an algorithm to estimate the Q_{PCB}, combining with equation (5), the above equations can be rewritten in state space form.

$$\begin{bmatrix} T_1^{k+1} \\ T_2^{k+1} \\ Q_{PCB}^{k+1} \end{bmatrix} = \begin{bmatrix} 1 - \frac{2K\Delta t}{C_M M_M} & \frac{2K\Delta t}{C_M M_M} & \frac{2K\Delta t}{C_M M_M} \\ \frac{2K\Delta t}{C_M M_M} & 1 - \frac{2K\Delta t}{C_M M_M} + k_3 & 0 \\ 0 & 0 & 1 \end{bmatrix} \begin{bmatrix} T_1^k \\ T_2^k \\ Q_{PCB}^k \end{bmatrix} -$$

$$\begin{bmatrix} 0 \\ \frac{2K\Delta t}{C_M M_M}\left(k_1 I_{TEM} - k_2 I_{TEM}^2 + k_3 T_2\right) \\ 0 \end{bmatrix}$$

$$(8)$$

$$y^k = \begin{bmatrix} 1 & 0 & 0 \end{bmatrix} \begin{bmatrix} T_1^k & T_2^k & Q_{PCB}^k \end{bmatrix}$$

$$(9)$$

EXPERIMENT

Experimental Setup

The lithium ion battery used for this study is a pouch type lithium ion battery with the dimensions about 20cm×15cm×5mm. The capacity is 15.7Ah and the operating voltage is from 2.5V to 4.15V. A test station was designed to charge/discharge the battery using a DC power supply and an electronic load, and to estimate the heat generation rate of lithium ion battery by TEMs, which are controlled by LabVIEW embedded in a PC, as shown in Figure 4 and Figure 5.

Current was measured by a high-resolution current sensor and the surface temperature was measured by two thermocouples placed at the center of the both sides of the battery surface.
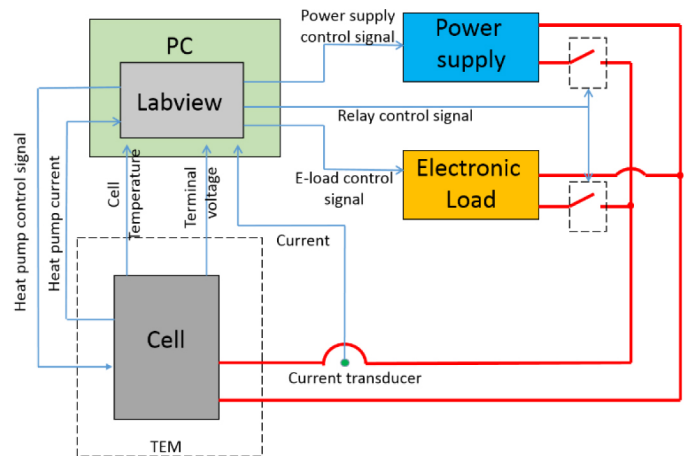

Figure 4. Experimental setup

Two TEMs were used to construct a thermal isolation room and heat was only pumped out by TEMs. PCB or battery was placed in the thermal isolation room between the two TEMs. In order to improve the heat conduction, carbon based thermal sheets were stuck to the metal plate, as shown in Figure 6. Two TEMs were connected in series and powered by a bipolar power supply controlled by LabVIEW.

A printed circuit board (PCB) with the same size as the battery was used as a dummy load to identify a set of thermal parameters and calibrate some unknown parameters. The resistance value of the PCB board is 0.5Ω, so the heat generation used as a reference value can be easily calculated at a given current using Ohm's law.
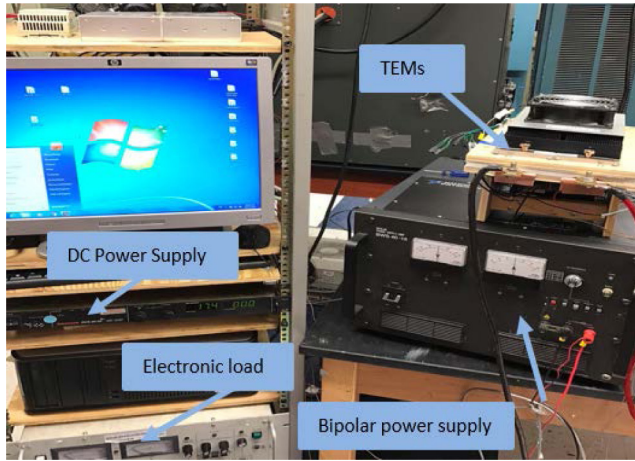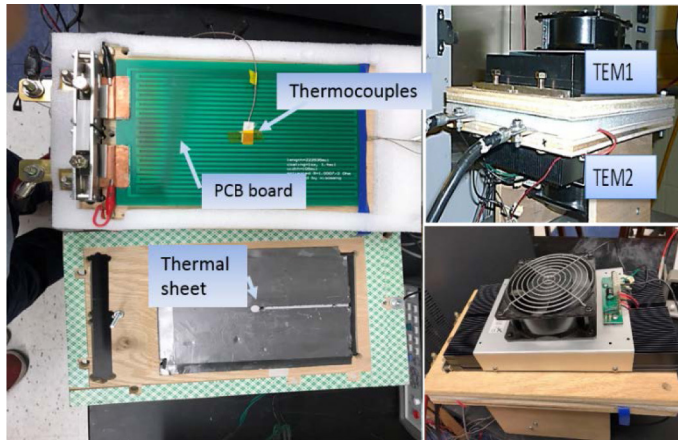

Figure 5. Designed test station

Figure 6. Calorimeter setup

Parameter Identification

After setting up the test station, parameter identification was conducted to acquire the relationship between the heat pumping rate and the input current of TEM, as in equation (5) and also identify the parameters of the model of metal plate, as in equation (6).

When the battery starts to generate heat and TEM starts to pump out the heat, there is a temperature gradient in the metal plate because of the heat capacity of the metal plate as depicted in Figure 2. The outside surface temperature of the metal plate, T_1, can be measured, however the inside temperature of the metal plate, T_2, cannot be

measured. In order to estimate T_2, the current flowing into PCB board was kept as constant, and the current flowing into TEM was adjusted to make that the final value of T_1 is equal to the initial value of T_1, which means the heat generation from PCB is equal to the heat pumped out by the TEMs and also means that the average temperature of the metal plate doesn't change, as plotted in Figure 7. The inside temperature of the metal plate T_2 is estimated by equation (10),

$$T_2 = 2 \cdot T_{initial} - T_{working}$$
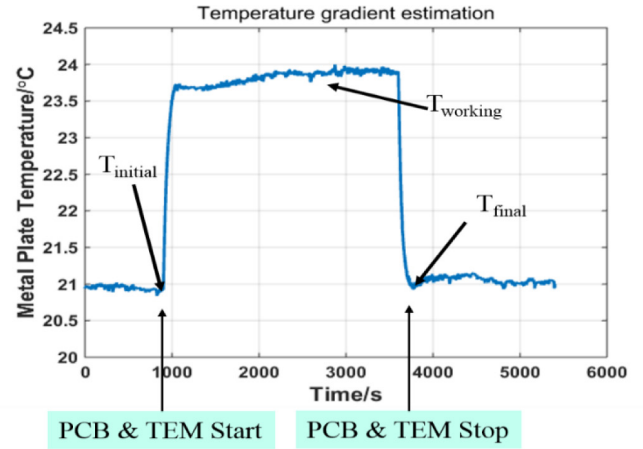
(10)

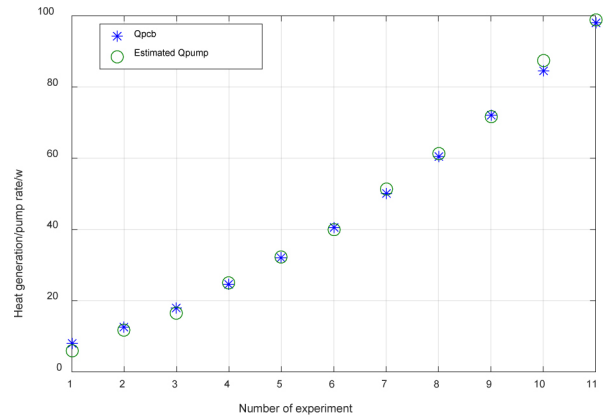Figure 7. Response of outside temperature of metal plate T_1.

Figure 8. Comparison of experiment values and estimation values.

Current flowing into PCB is adjusted to get different heat generation rate and then repeat the above process to find different sets of values of Q_{pump}, I_{TEM}, T_2 and T_3, T_4. Temperature T_3 that cannot be measured, is assumed to be equal to T_4 because when TEM works, the temperature T_4 is very high and the distance between T_3 and T_4 is very short.

After getting the data above, the least square method was used to find the coefficients k_1, k_2, k_3 in equation (11). The results of experiment and estimation are shown in Figure 8, which indicates that the identified coefficients are close to the measured values.

$$Q_{pump} = 0.166 \cdot T_2 \cdot I_{TEM} - 4.587 \cdot I_{TEM}^2 - 1.5 \cdot (T_2 - T_3)$$

(11)

From equation (6), we get

$$T_1 = \frac{0.5 * C_M M_M \dot{T}_2 + K_1 T_2 + Q_{Pump}}{K_1}$$

$$\dot{T}_1 = \frac{0.5 * C_M M_M \ddot{T}_2 + K_1 \dot{T}_2 + \dot{Q}_{Pump}}{K_1}$$

(12)

Substituting equation (12) into equation (6),

$$Q_{PCB} - (0.5 * C_M M_M \dot{T}_2 + K_1 T_2 + Q_{Pump}) + K_1 T_2 =$$
$$\frac{(0.5 * CM)^2 \ddot{T}_2 + 0.5 * K_1 C_M M_M \dot{T}_2 + \dot{Q}_{Pump}}{K_1}$$

(13)

When $Q_{PCB} = Q_{pump}$ and $\dot{Q}_{PCB} = 0$,

$$\frac{(0.5 * C_M M_M)^2}{K_1} \ddot{T}_2 + C_M M_M \dot{T}_2 - Q_{PCB} + Q_{pump} + \frac{\dot{Q}_{Pump}}{K_1} = 0$$

(14)

$$T_2(t) = C_1 e^{r_1 t} - C_2 e^{r_2 t}$$

(15)

In the same way, we can get

$$T_1(t) = C_1 e^{r_1 t} + C_2 e^{r_2 t}$$

(16)

Where $r_1 = 0$ and $r_2 = -\dfrac{4K_1}{C_M M_M}$

When the TEM is in a steady state, T_1 and T_2 do not change with respect to time.

$$Q_{PCB} = K_1(T_1 - T_2)$$

(17)

$$T_1 - T_{amb} = T_{amb} - T_2$$

(18)

where T_{amb} is the ambient temperature. Substituting equation (18) into equation (17), we obtain

$$K_1 = \frac{Q_{PCB}}{2(T_1 - T_{amb})}$$

(19)

Q_{PCB} is calculated by Ohm's law and T_1 and T_{amb} are measured by the thermal couples. Figure 7 shows the temperature of T_1 measured by the thermal couples. Based on equation (16), the least square method is used to identify the parameter K_1 and $C_M M_M$.

In order to validate the identified results, the simulation results using the identified value are compared with experiment data, as shown in Figure 9. Zoomed-in views of the transient behaviors are shown in Figure 10. The results show that the identified values are close to experimental values of the system.

Design of Kalman filter

Kalman filter proposed by R.E. Kalman is a recursive dynamic estimator to solve the linear quadratic problem. The method is applied to estimate instantaneous states of a linear dynamic system perturbed by white noises. The resulting estimation is statistically optimal with respect to any quadratic function of estimation errors [27].
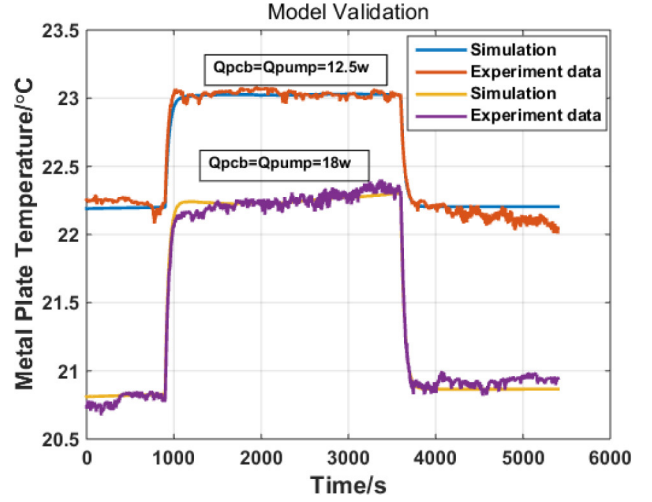

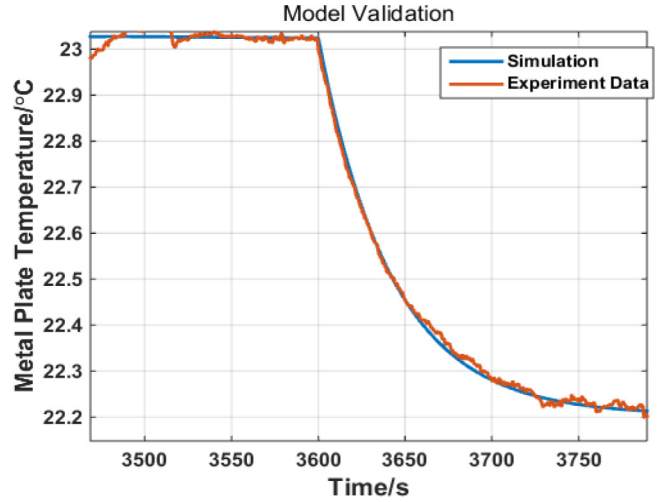Figure 9. Model validation

Figure 10. Expanded views of the transient behaviors

Application of Kalman filter requires state space equations for state and measurement equation. State space representation with difference equations of Kalman filter is written as (20)-(21). The random variables, w_k and v_k represent the process and measurement noises, respectively, which are assumed to be Gaussian white noise that has a normal probability, shown in equations (22). In this paper, the state space equation of the calorimeter is derived as (8)-(9).

$$x_k = A x_{k-1} + B u_k + w_k$$

(20)

$$z_k = H \cdot x_k + v_k$$

(21)

$$E(w_k w_i^T) = \begin{cases} Q_k, i = k \\ 0, i \neq k \end{cases} \qquad E(v_k v_i^T) = \begin{cases} R_k, i = k \\ 0, i \neq k \end{cases} \qquad E(w_k v_i^T) = 0,$$

$$(22)$$

The state updated by Kalman filter are shown in Figure 11. The diagonal values of the covariance matrix are 10^{-4}, 10^{-4} and 10^{-2}. The value of the measurement covariance is 10^{-2}.

Enter Prior estimate $\hat{\mathbf{X}}_0$ @k=1

And its error covariance P_0

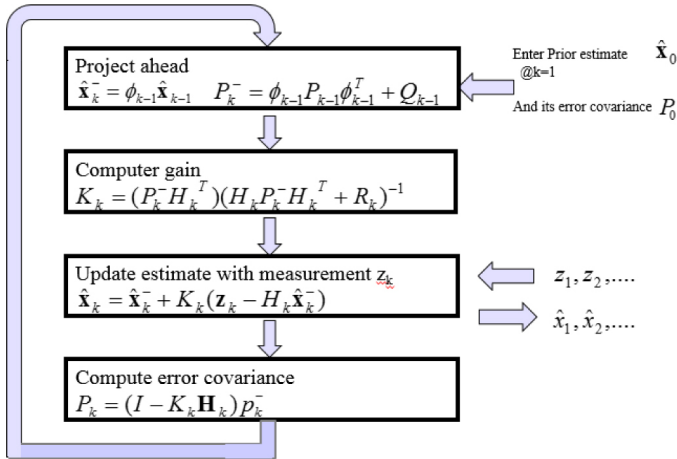$z_1, z_2, \ldots$

$\hat{x}_1, \hat{x}_2, \ldots$

Figure 11. Kalman filter working process.

Design of Controller

The block diagram for the temperature control loop is shown in Figure 12. The temperature of the surface of the object is measured and compared with the reference value. The difference is amplified to control the input current of TEM to keep the heat pump rate of TEM following the variation of heat generation rate of the object (battery or PCB) and also keep the temperature as constant. The function $f(I_{TEM})$ is nonlinear, as shown in equation (5), which is linearized by applying the method of inverse nonlinearity, $f(\hat{Q}_{pump})$.

By Laplace transform, the transfer functions of the metal plate is given in equation (23). Five different types of classical controller were designed and optimized by comparison of their performances. By simulation, the lead-lag compensator was the best controller, as shown in Figure 13.
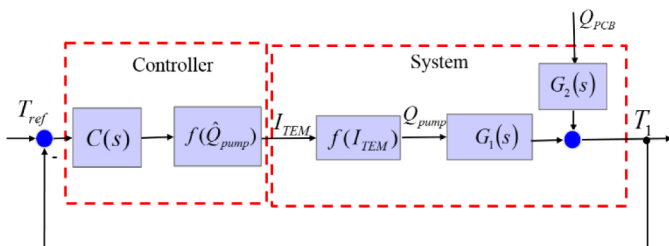

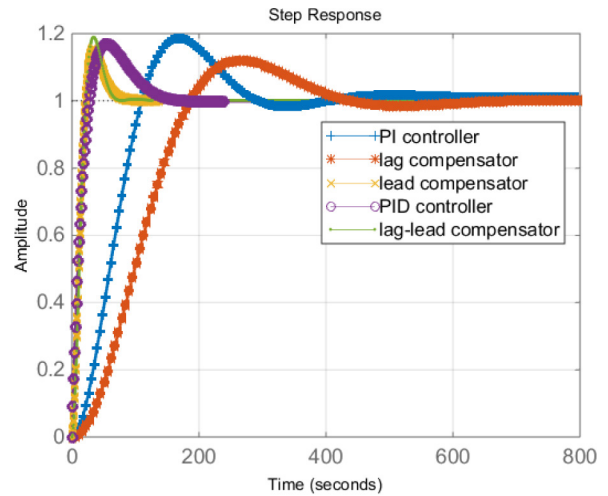Figure 12. Block diagram of controller

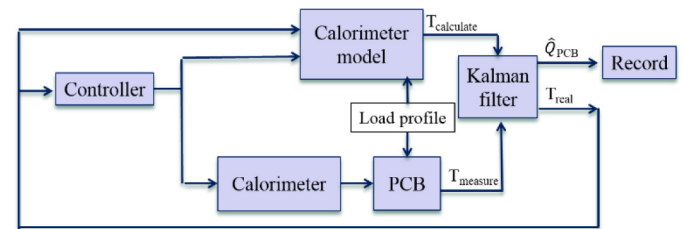Figure 13. Step response of different controller by simulation.

Figure 14. Schematic diagram for estimation of heat generation of PCB

$$G_1(s) = \frac{T_1(s)}{Q_{pump}(s)} = -\frac{K}{C_M M_M{}^2 S^2 + 2 C_M M_M K S^2}$$

$$G_2(s) = \frac{T_1(s)}{Q_{PCB}(s)} = \frac{K}{C_M M_M{}^2 S^2 + 2 C_M M_M K S^2}$$

$$(23)$$

RESULTS AND DISCUSSION

A thermal model of the calorimeter was developed and a controller was designed and optimized based on experiments. PCB board was used as a dummy load to identify the parameters of the model and finish the static and dynamic calibration. The heat generation rate was estimated by Kalman filter. The schematic diagram for estimation of heat generation rate of PCB or battery and control of the temperature of PCB as well as battery is shown in Figure 14.

At first, the heat generation estimation algorithm was validated by simulation in Simulink/MATLAB. The heat generation rate of PCB was set up at 40W and then the temperature T_1, T_2, I_{TEM} were recorded by simulation, as shown in Figure 15. Then, those data were used to validate the designed heat generation estimation algorithm. The results are shown in Figure 16. The simulation results show that the designed algorithm works well. It takes about 90 seconds to track the heat generation of PCB. After the convergence of Kalman filter, the estimated heat generation rate is the same as that of the simulation. The error is less than 0.1W.

After simulation, the designed heat generation algorithm is validated against experimental data. The heat generation rate of PCB was set as 10W, 20W, 30W, 40W and 50W through the power supply controlled by LabVIEW. Kalman filter was used to estimate the heat generation rate of PCB. Results are shown in Figure 17, where two heat generation rate are plotted. The one from the PCB given by Ohm's law (brown line) and another one from the calorimeter estimated by Kalman filter (blue line). The expanded views of the transient behaviors are shown at the right side of the plot. The proposed method provides an outstanding tracking performance of heat generation rate of PCB. It takes about 100 seconds to catch up, which is almost the same as the simulation results. The average error of estimated heat generation rate is less than 2W, shown in Table 1.

Another purpose of the designed TEM is to control the temperature of PCB as constant. In order to validate the performance of the designed controller, the heat generation rate of PCB was controlled as 10W, 20W, 30W, 40W, 50W to confirm if the TEM can keep the temperature of PCB as constant. The temperature of PCB is shown in Figure 18, where the designed controller has relatively good performance. It takes about 200 seconds to keep the temperature of PCB to be constant. The average error of temperature is less 1°C, shown in Table 1.

Table 1. The average error of estimated heat generation rate and temperature of PCB.

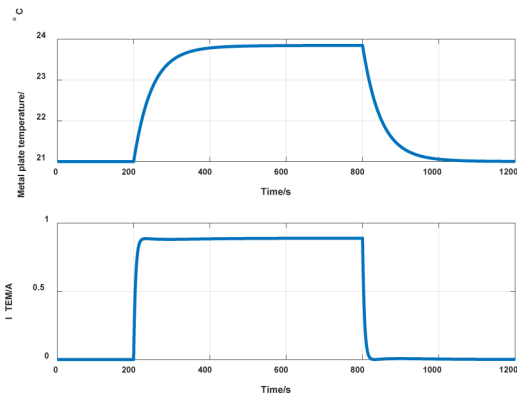| Heat generation rate of PCB (W)	10	20	30	40	50
Average error of estimated heat (W)	0.5	1	1.1	1.5	1.6
Average error of temperature(°C)	0.2	0.3	0.35	0.36	0.5

Figure 15. Simulation results of metal plate temperature and the input current of TEM
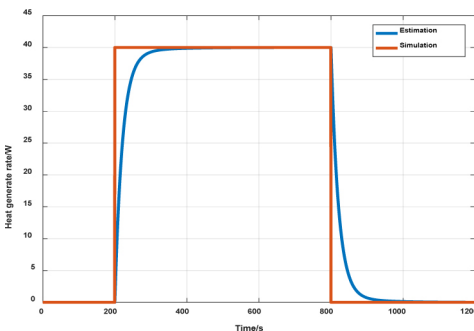

Figure 16. Simulation results of heat generation.
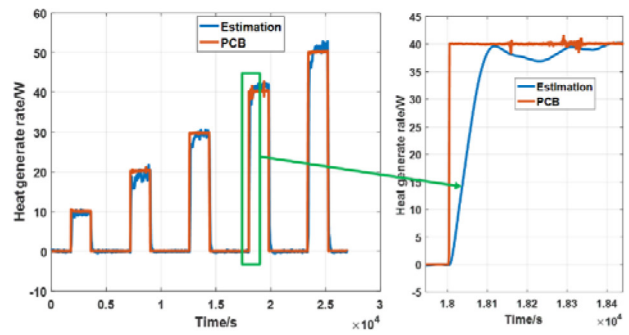

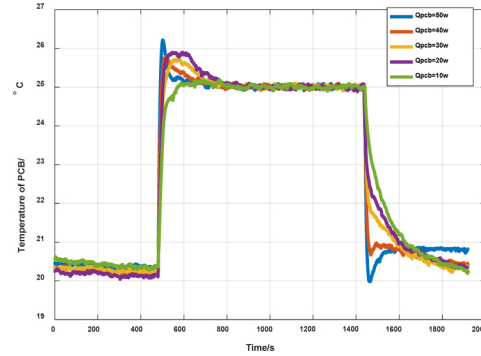Figure 17. Estimation results of heat generation rate

Figure 18. Temperature of PCB

The tests above show validation of the designed calorimeter using the PCB board. Finally, the designed calorimeter is used to measure the heat generation of the battery.

The reversible heat generation is the change of entropy at a given temperature and can be obtained using the change of open circuit voltage (OCV) over temperature, as shown in equation (24).

$$Q_{rev} = -I \cdot T \cdot \frac{\partial U_{OCV}}{\partial T}$$

(24)

where I is the charging or discharging current, which sign is defined as positive when discharged. T is the temperature in the battery and U_{OCV} is the open circuit voltage.

The irreversible heat source is determined by the difference between the terminal voltage and open circuit voltage at a given current,

$$Q_{irr} = I \cdot (U_{OCV} - V_t)$$

(25)

where V_t is the terminal voltage.

The above equation becomes zeros when the current is zero. In fact, heat is continuously generated during resting after charging or discharging, which is caused by the gradient of ion concentration and is called the heat of mixing. However, the value of heat mixing is relatively small compared with irreversible and reversible heat sources [1], so the heat of mixing is not considered in this paper.

Current and terminal voltage can be measured directly and state of charge (SOC) can be calculated by coulomb counting. *OCV* can be calculated by the equation *OCV=f(SOC)*, which can be determined experimentally. $\frac{\partial U_{OCV}}{\partial T}$ is assumed as a constant value 2.2×10-4 V/K [28].

The total heat generation of the battery was measured when the battery was charging or discharging at different currents. The measured and simulated results are shown in Figure 19 and Figure 20. The solid lines show the heat generation rate measured by the designed calorimeter and the dashed line show the simulated results.
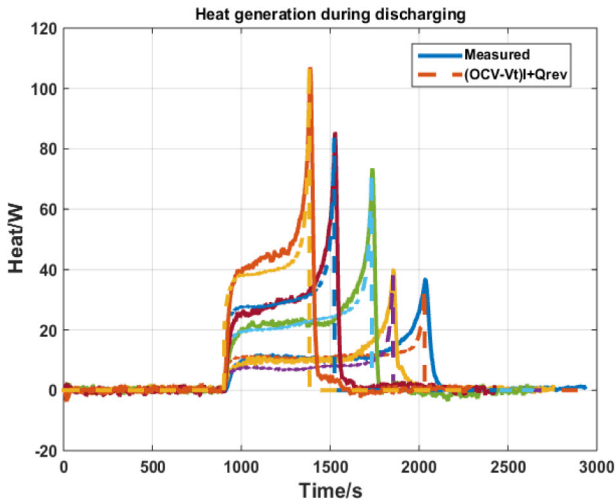

Figure 19. Comparison between measured results and simulated results at discharging
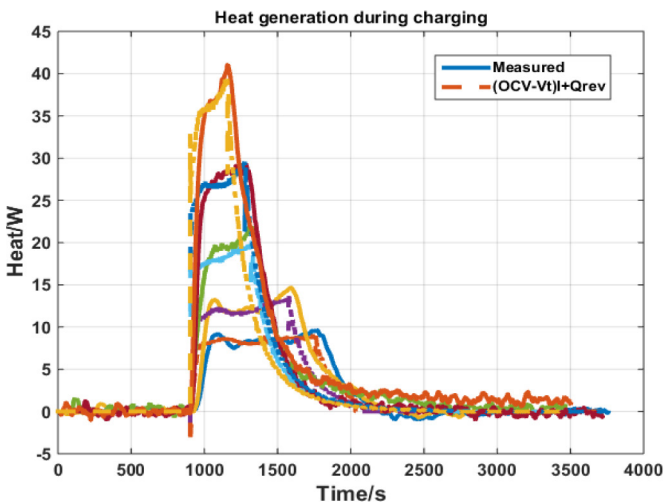

Figure 20. Comparison between measured results and simulated results at charging

Table 2. Average error of estimated heat generation rate for battery

Discharging current (A)	46.8	54.6	62.4	78	93.6
Average error of estimated heat (W)	2.16	2.35	2.46	2.49	2.6
Charging current (A)	46.8	54.6	62.4	78	93.6
Average error of estimated heat (W)	2.25	2.32	2.41	2.45	2.56

The figures show that the designed calorimeter has a good tracking performance in the measurement of heat generation rate of the battery. The average error of the estimated heat generation rate is less than 3W, as summarized in Table 2.

CONCLUSIONS

In this works, we proposed a highly dynamic calorimeter that can be used to characterize the thermal behaviors of a pouch type of lithium ion battery. Estimation of the heat generation rate needed a thermal model of the TEM, which parameters were extracted using a PCB. At the same time, the PCB was used to calibrate the static and dynamic responses. Based on the thermal model of the calorimeter, Kalman filter was designed to improve the dynamic response of TEM. By experiment validation, our designed heat generation estimation method works well and can track the variation of heat generation of PCB. It takes about 100 seconds for designed algorithm to follow the changing of heat generation rate of PCB. The average error of estimated heat generation rate is less than 2W. The designed controller also has good performance and the temperature of PCB can be kept as constant, which takes about 200 seconds. The average error of temperature is less than 1°C. Battery testing data also show that the designed calorimeter has good tracking performance for the measurement of heat generation rate of the battery. The average error of the estimated heat generation rate is less than 3W.

Although the obtained results are satisfactory for thermal performance, some issues must be investigated further, namely, (i) reduction the estimation error of heat generation rate;(ii) improvement of the convergence speed of Kalman filter; (iii), increase of the measurement frequency; (iv) optimization of the controller to improve the temperature response of calorimeter.

REFERENCES

1. Xiao, M. and Choe, S., "Dynamic modeling and analysis of a pouch type LiMn 2 O 4/Carbon high power Li-polymer battery based on electrochemical-thermal principles." *Journal of Power Sources* 218 (2012): 357–367, dio:10.1016/j.jpowsour.2012.05.103.

2. Santhanagopalan, S., Zhang, Q., Kumaresan, K. and White, R.E., Parameter estimation and life modeling of lithium-ion cells." *Journal of The Electrochemical Society* 155, no. 4 (2008): A345–A353, dio:10.1149/1.2839630

3. Awarke, A., Jaeger, M., Oezdemir, O. and Pischinger, S., "Thermal analysis of a Li ion battery module under realistic EV operating conditions." *International Journal of Energy Research* 37, no. 6 (2013): 617–630. dio: 10.1002/er.2884

4. Bhide, S. and Shim, T., "Novel predictive electric Li-ion battery model incorporating thermal and rate factor effects." *IEEE Transactions on vehicular technology* 60, no. 3 (2011): 819–829. dio:10.1109/TVT.2010.2103333

5. Yang K., An J.J., Chen S., "Temperature characterization analysis of LiFePO4/C power battery during charging and discharging." *Journal of thermal analysis and calorimetry* 99, no. 2 (2010): 515–521. dio:10.1007/s10973-009-0623-1

6. Bernardi, D., Pawlikowski, E. and Newman, J., Bernardi, D., Pawlikowski E., and Newman John. "A general energy balance for battery systems." *Journal of the electrochemical society* 132, no. 1 (1985): 5–12, dio: 10.1149/1.2113792.

7. Smith, K. and Wang, C.Y., "Power and thermal characterization of a lithium-ion battery pack for hybrid-electric vehicles." *Journal of power sources* 160, no. 1 (2006): 662–673, dio: 10.1016/j.jpowsour.2006.01.038

8. Gu, W.B. and Wang, C.Y., "Thermal-Electrochemical Modeling of Battery Systems." *Journal of The Electrochemical Society* 147, no. 8 (2000): 2910–2922, dio:10.1149/1.1393625

9.   Wang, C.Y. and Srinivasan, V., "Computational battery dynamics (CBD)—electrochemical/thermal coupled modeling and multi-scale modeling." *Journal of power sources* 110, no. 2 (2002): 364–376, dio:10.1016/S0378-7753(02)00199-4.

10. Chen, K., Unsworth, G. and Li, X., "Measurements of heat generation in prismatic Li-ion batteries." *Journal of Power Sources* 261 (2014): 28–37, dio:10.1016/j.jpowsour.2014.03.037

11. Forgez, C., Do, D.V., Friedrich, G., Morcrette, M., , "Thermal modeling of a cylindrical LiFePO 4/graphite lithiumion battery." *Journal of Power Sources* 195, no. 9 (2010): 2961–2968, dio:10.1016/j.jpowsour.2009.10.105.

12. Hong, J.S., Maleki, H., Al Hallaj, S., Redey, L., "Electrochemical-calorimetric studies of lithium ion cells." *Journal of the Electrochemical Society* 145, no. 5 (1998): 1489–1501, dio:10.1149/1.1838509

13. Song, L. and Evans, J.W., "Electrochemical Thermal Model of Lithium Polymer Batteries." *Journal of the Electrochemical Society* 147, no. 6 (2000): 2086–2095, dio:10.1149/1.1393490

14. Kim, J.S., Prakash, J. and Selman, J.R., "Thermal Characteristics of Li x Mn2 O 4 Spinel." *Electrochemical and solid-state letters* 4, no. 9 (2001): A141–A144.

15. Guiatni, M. and Kheddar, A., "Modeling identification and control of peltier thermoelectric modules for telepresence." *Journal of Dynamic Systems, Measurement, and Control* 133, no. 3 (2011): 031010, dio:10.1115/1.4003381.

16. Ciccarella, G. and Marietti, P., "Model reference adaptive control of a thermostatic chamber." *IEEE Transactions on Industrial Electronics* 36, no. 1 (1989): 88–93. dio:10.1109/41.20352

17. Schutze, J., Ilgen, H. and Fahrner, W.R., "An integrated micro cooling system for electronic circuits." *IEEE transactions on industrial electronics* 48, no. 2 (2001): 281–285, dio:10.1109/41.915406

18. Hodes, M., "Optimal pellet geometries for thermoelectric refrigeration." *IEEE Transactions on Components and Packaging Technologies* 30, no. 1 (2007): 50–58, doi:10.1109/TCAPT.2007.892068

19. Lau, P.G. and Buist, R.J., "Temperature and time dependent finite-element model of a thermoelectric couple." In *Thermoelectrics, 1996., Fifteenth International Conference on*, pp. 227–233. IEEE, 1996, dio: 10.1109/ICT.1996.553305.

20. Seifert, W., Ueltzen, M., Strumpel, C., Heiliger, W. , "One dimensional Modelling of Thermoelectric Cooling." physica status solidi (a) 194, no. 1 (2002): 277–290, dio: 10.1002/1521-396X(200211)194:1<277::AID-PSSA277>3.0.CO;2-5.

21. Neto, A., Almeida, L., Lima, A., Deep, G., "Recursive arma modeling for thermoelectric modules." In *Instrumentation and Measurement Technology Conference, 2003. IMTC'03. Proceedings of the 20th IEEE*, vol. 2, pp. 919–923. IEEE, 2003. dio:0.1109/IMTC.2003.1207887

22. Carslaw, H. S., Jaeger, J. C., "Conduction of Heat in Solids, Clarendon Press", Oxford, 1959.

23. Labudovic, M. and Li, J., "Modeling of TE cooling of pump lasers." *IEEE Transactions on components and packaging technologies* 27, no. 4 (2004): 724–730, dio:10.1109/TCAPT.2004.838874

24. Chen, J., Yan, Z. and Wu, L., "Nonequilibrium thermodynamic analysis of a thermoelectric device." *Energy* 22, no. 10 (1997): 979–985, dio: 10.1016/S0360-5442(97)00026-1.

25. Hodes, M., "On one-dimensional analysis of thermoelectric modules (TEMs)." *IEEE Transactions on Components and packaging technologies* 28, no. 2 (2005): 218–229, dio: 10.1109/TCAPT.2005.848532.

26. Lineykin, S. and Ben-Yaakov, S., "Modeling and analysis of thermoelectric modules." *IEEE Transactions on Industry Applications* 43, no. 2 (2007): 505–512, dio:10.1109/TIA.2006.889813

27. Grewal, M.S., Andews, A. P., "Kalman Filtering: Theory and Practice Using MATLAB", John Wiley & Sons, Inc, 2001.

28. Song, L. and Evans, J.W., "Electrochemical thermal model of lithium polymer batteries." *Journal of the Electrochemical Society* 147, no. 6 (2000): 2086–2095.

CONTACT INFORMATION

Corresponding Contact: Song-yul Choe

Mailing address: 1418 Wiggins hall, Auburn UniversityAuburn AL, 36849

choeson@auburn.edu

DEFINITIONS/ABBREVIATIONS

EV - Electric vehicle

C - Accelerated-rate calorimetry

IHC - Heat conduction calorimetry

PCB - Printed circuit board

SOC - State of Charge

OCV - Open circuit voltage

Q_{pump} - heat pump rate of calorimeter

I_{TEM} - Input current of TEM

T_2, T_3 - Temperature on both sides of TEM

T_1 - Outside surface temperature of metal plate

T_4 - Temperature of heat sink

K - Thermal conductivity

C_M - Heat capacity of metal plate

M_M - Mass of metal plate

Q_{PCB} - Heat generated by the PCB board

α - Seebeck coefficient

τ - Thomson coefficient

k_1 - Peltier coefficient

k_2 - Resistance of TEM

k_3 - Thermal conduction

T_{amb} - Ambient temperature

w_k - Process noise at sampling time k

v_k - Measurement noise at sampling time k

Q_k, R_k - Covariance matrix.

Q_{tot} - Total heat generation rate of battery

Q_{rev} - Reversible heat source

Q_{irr} - Irreversible heat source